

Article

A Stability Analysis of Solutions in Boundary Layer Flow and Heat Transfer of Carbon Nanotubes over a Moving Plate with Slip Effect

Nur Syazana Anuar ^{1,*} , Norfifah Bachok ^{1,2} and Ioan Pop ³

¹ Department of Mathematics, Faculty of Science, Universiti Putra Malaysia, UPM Serdang, Selangor 43400, Malaysia; norfifah@upm.edu.my

² Institute for Mathematical Research, Universiti Putra Malaysia, UPM Serdang, Selangor 43400, Malaysia

³ Department of Mathematics, Babes-Bolyai University, 400084 Cluj-Napoca, Romania; popm.ioan@yahoo.co.uk

* Correspondence: nursyazana931@gmail.com; Tel.: +60-17-221-8001

Received: 30 September 2018; Accepted: 16 November 2018; Published: 22 November 2018



Abstract: The flow and heat transfer characteristics of both single-wall and multi-wall carbon nanotubes (CNTs) with water and kerosene as base fluid on a moving plate with slip effect are studied numerically. By employing similarity transformation, governing equations are transformed into a set of nonlinear ordinary equations. These equations are solved numerically using the *bvp4c* solver in Matlab which is a very efficient finite difference method. The influence of numerous parameters such as nanoparticle volume fraction, velocity ratio parameter and first order slip parameter on velocity, temperature, skin friction and heat transfer rate are further explored and discussed in the form of graphical and tabular forms. The results reveal that dual solutions exist when the plate and free stream move in the opposite direction and slip parameter was found to widen the range of the possible solutions. However, skin friction coefficients decrease, whereas the heat transfer increases in the presence of slip parameter. Single-wall carbon nanotubes (SWCNTs) give higher skin friction and heat transfer compared to multi-wall carbon nanotubes (MWCNTs) due to the fact that they have higher density and thermal conductivity. A stability analysis is carried out to determine the stability of the solutions obtained.

Keywords: stability analysis; carbon nanotubes; heat transfer; moving plate; slip effect

1. Introduction

In the past few decades, the thermal conductivity of nanofluids has been investigated by many researchers. Most of the studies on nanofluids are about understanding their behaviors so that they can optimize the enhancement of heat transfer in many industrial applications; i.e., nuclear reactors, power generation, transportation, the cooling and drying of paper, electronics, biomedicine and food. A good list of applications is available in Das et al. [1]. It may be noted that nanometer-sized metallic particles are an important physical parameter that can improve the heat transfer of fluids. Choi and Estman [2] were the first to introduce the word nanofluids; they defined a nanofluid as a liquid containing dispersed submicronic solid particles (nanoparticles). While plenty of materials can be used to form nanoparticles, carbon shows promising results because of its high thermal, electrical and mechanical properties [3]. Thus, Choi et al. [4] studied the thermal conductivity of oil-based carbon nanotubes. They reported that dispersion of a very small amount of nanotubes (1 vol %) produced an outstanding increase in the thermal conductivity of the base fluid. Carbon nanotubes (CNTs) are cylindrical shaped carbon atom structures with diameters ranging between 1 and 50 nm. Carbon

nanotubes can consist of single-wall (SWCNTs) and multi-wall (MWCNTs) carbon nanotubes. Carbon nanotube suspensions offer higher thermal properties compared to those other nanoparticles with the same volume fraction [5,6]. Therefore, CNTs are able to enhance convective heat transfer performance and thermal conductivity of base fluids. Garg et al. [7] explored the influence of dispersing energy on viscous and heat transfer characteristic of MWCNTs dispersed in water whereby he noticed a 20% enhancement in the thermal conductivity. After that, many researchers have discovered the benefit of CNTs in their respective fields of study [8–10].

Blasius in 1908 [11] was most likely the first researcher to investigate the problem of boundary layer flow in a viscous fluid over a stationary flat plate. Wang [12] employed a new algorithm which known as a domain decomposition method to solve the classical Blasius equations. Later, Cortell [13] numerically investigated the classical Blasius flat-plate problem using the Runge-Kutta algorithm. Different from Blasius flow, Sakiadis [14] investigated the boundary layer flow over a continuous solid surface moving with constant velocity. Since then, many researchers [15–17] have considered the flow on a moving or fixed flat plate and reported that a duality exists for the case when the plate opposes the directions of the free stream.

In all previous studies, researchers only analyzed the flow field that only obeys the no-slip boundary condition. However, it is essential to substitute no-slip assumptions with partial slip boundary conditions as the former is not consistent with some practical flow situations. Bhattacharyya et al. [18,19] investigated the boundary layer slip flow over a flat plate with uniform magnetic field and considered the plate immersed into the porous medium. Later, Bhattacharyya et al. [20] studied the flow on moving flat plate in a parallel free stream with slip effect. Bachok et al. [21] generalized this idea and extended the problem to a moving plate in a copper-water nanofluid. Nevertheless, the above problems have not dealt with carbon nanotubes. Khan et al. [22] was the first to consider the flow and heat transfer of carbon nanotubes along a flat plate by employing a homogeneous flow model subjected to Navier slip and uniform heat flux boundary conditions. Various boundary layer flow problem of carbon nanotubes has also been also investigated by many authors [23–26].

The main focus here is to extend the research done by Bachok et al. [21]. This research is different from the previous related work in the sense that here we utilize the concept of carbon nanotubes consisting of water and kerosene-based nanofluid SWCNTs and MWCNTs introduced by Khan et al. [22] and the carbon nanotube model used for this research is taken from Xue [8]. Additionally, the flow considered in [22] is for a stationary plate, whereas this research considers the problem over a moving plate. We also implemented the stability analyses reported by Merkin [27], Weidman et al. [28], Merrill et al. [29] and Harris et al. [30]. We believe that this case has not been reported in any of the previous literature.

2. Problem Formulation

Consider a two-dimensional, steady and incompressible flow past a moving plate in a water and kerosene base fluid containing single-wall and multi-wall carbon nanotubes (CNTs) as a nanoparticle. A Cartesian coordinate system is used with the x -axis along the plate and the y -axis perpendicular to the plate. Further, we assume that the plate is maintained at uniform temperature T_w and T_∞ corresponds to the ambient fluid temperature. It is assumed that the plate moves with a constant velocity U_w and U_∞ corresponds to the free stream velocity far from the surface of the plate. The physical model is depicted in Figure 1. The boundary layer equations can be written as [21]:

$$\frac{\partial u}{\partial x} + \frac{\partial v}{\partial y} = 0 \quad (1)$$

$$u \frac{\partial u}{\partial x} + v \frac{\partial u}{\partial y} = \frac{\mu_{nf}}{\rho_{nf}} \frac{\partial^2 u}{\partial y^2} \quad (2)$$

$$u \frac{\partial T}{\partial x} + v \frac{\partial T}{\partial y} = \alpha_{nf} \frac{\partial^2 T}{\partial y^2} \tag{3}$$

and the boundary conditions are defined as follows:

$$\begin{aligned} u &= U_w + L_1 \left(\frac{\partial u}{\partial y} \right), v = 0, T = T_w \text{ at } y = 0 \\ u &\rightarrow U_\infty, T \rightarrow T_\infty \text{ as } y \rightarrow \infty \end{aligned} \tag{4}$$

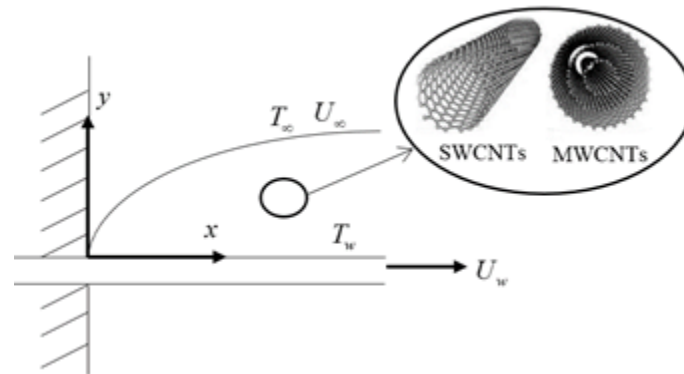


Figure 1. Schematic diagram of the problem.

The velocity components in x and y directions are namely u and v , T is the temperature, L_1 is the slip factor, μ, α and ρ is the dynamic viscosity, thermal diffusivity and density where the subscripts ' nf ', ' f ' and ' CNT ' represent 'nanofluid', 'fluid' and 'carbon nanotube', respectively. The slip factor are defined as $L_1 = L(\text{Re}_w + \text{Re}_\infty)^{1/2}$ where L is the initial length of slip factor, $\text{Re}_w = U_w x / \nu_f$ is the Reynolds number based on the plate velocity and $\text{Re}_\infty = U_\infty x / \nu_f$ is the Reynolds numbers based on the free stream velocity, respectively. The effective properties of nanofluids are given by [31]:

$$\begin{aligned} \alpha_{nf} &= \frac{k_{nf}}{(\rho C_p)_{nf}}, \mu_{nf} = \frac{\mu_f}{(1-\phi)^{2.5}}, \rho_{nf} = (1-\phi)\rho_f + \phi\rho_{CNT}, \\ (\rho C_p)_{nf} &= (1-\phi)(\rho C_p)_f + \phi(\rho C_p)_{CNT}, \\ \frac{k_{nf}}{k_f} &= \frac{1-\phi+2\phi \frac{k_{CNT}}{k_f} \ln \frac{k_{CNT}+k_f}{2k_f}}{1-\phi+2\phi \frac{k_f}{k_{CNT}-k_f} \ln \frac{k_{CNT}+k_f}{2k_f}} \end{aligned} \tag{5}$$

where (ρC_p) is the heat capacity, ϕ is the nanoparticle volume fraction and k is the thermal conductivity, respectively. The use of the term for k_{nf}/k_f were taken from Xue [8] where the model based on Maxwell theory considering the effect of space distribution of CNTs on thermal conductivity. Thermophysical properties for different base fluids are listed in Table 1.

Table 1. Thermophysical properties of CNTs (Khan et al. [22]).

| Physical Properties | Base Fluids | | Nanoparticle | |
|-----------------------------|------------------|--------------------|--------------|-------|
| | Water (Pr = 6.2) | Kerosene (Pr = 21) | SWCNT | MWCNT |
| ρ (kg/m ³) | 997 | 783 | 2600 | 1600 |
| c_p (J/kg K) | 4179 | 2090 | 425 | 796 |
| k (W/m K) | 0.613 | 0.145 | 6600 | 3000 |

Similarity solutions of Equations (1)–(4) are presented in the following form:

$$\eta = \left(\frac{U}{v_f x} \right)^{\frac{1}{2}} y, \psi = (v_f x U)^{\frac{1}{2}} f(\eta), \theta(\eta) = \frac{T - T_\infty}{T_w - T_\infty} \tag{6}$$

where the composite velocity, U is defined as $U = U_w + U_\infty$. Afzal et al. [32] was the first who introduced this definition of U . ψ represents the stream function and defined as $u = \partial\psi/\partial y$ and $v = -\partial\psi/\partial x$ which identically satisfy Equation (1). By substituting Equation (6) into Equations (2) and (3), then we have:

$$\frac{1}{(1-\varphi)^{2.5} \left(1 - \varphi + \varphi \rho_{CNT} / \rho_f\right)} f''' + \frac{1}{2} f f'' = 0 \quad (7)$$

$$\frac{1}{Pr} \frac{k_{nf}/k_f}{\left[1 - \varphi + \varphi (\rho C_p)_{CNT} / (\rho C_p)_f\right]} \theta'' + \frac{1}{2} f \theta' = 0 \quad (8)$$

The original boundary condition (4) now takes the following form:

$$\begin{aligned} f(0) = 0, f'(0) = \lambda + \sigma f''(0), \theta(0) = 1 \\ f'(\eta) \rightarrow 1 - \lambda, \theta(\eta) \rightarrow 0 \text{ as } \eta \rightarrow \infty \end{aligned} \quad (9)$$

Here, primes denote the differentiation with respect to η . Pr is the Prandtl number, λ is the velocity parameter and σ is the slip parameter, which are defined as:

$$Pr = \frac{\nu_f}{\alpha_f}, \lambda = \frac{U_w}{U}, \sigma = L \frac{U}{\nu_f} \quad (10)$$

where, ν_f is the kinematic viscosity. Note that, $\lambda > 0$ represents the plate move in assisting flow, while $\lambda < 0$ represents the plate move in opposing flow [17]. It is worth mentioning that in the absence of CNTs ($\varphi = 0$) and slip parameter ($\sigma = 0$), the present problem reduces to those considered by Blasius [11] when $\lambda = 0$, and Sakiadis [14] when $\lambda = 1$.

The skin friction coefficient C_f and the local Nusselt number Nu_x , defined as:

$$C_f = \frac{\tau_w}{\rho_f U^2}, Nu_x = \frac{x q_w}{k_f (T_w - T_\infty)} \quad (11)$$

where τ_w and q_w is the surface shear stress and heat flux which are given by:

$$\tau_w = \mu_{nf} \left(\frac{\partial u}{\partial y} \right)_{y=0}, q_w = -k_{nf} \left(\frac{\partial T}{\partial y} \right)_{y=0} \quad (12)$$

using Equation (6) in (11) and (12), we obtain:

$$C_f Re_x^{1/2} = \frac{1}{(1-\varphi)^{2.5}} f''(0), Nu_x Re_x^{-1/2} = -\frac{k_{nf}}{k_f} \theta'(0) \quad (13)$$

where $Re_x = Ux/\nu_f$ is the local Reynolds number.

3. Flow Stability

It is important to determine the physical reliability of dual solutions obtain because there is more than one solution. A further question that will arise later is which solutions are physically acceptable solutions and have physical meanings. Hence, we now investigate the stability of the solutions obtained using Equations (7) and (8) subject to the boundary conditions (9) to determine which solution is stable and physically realizable and which is not stable. These features are tested by

first considering the time-dependent problem (see Merkin [27]) due to the fact that there exists a small perturbation to the solutions. Equation (1) holds, while Equations (2) and (3) are replaced by:

$$\frac{\partial u}{\partial t} + u \frac{\partial u}{\partial x} + v \frac{\partial u}{\partial y} = \frac{\mu_{nf}}{\rho_{nf}} \frac{\partial^2 u}{\partial y^2} \quad (14)$$

$$\frac{\partial T}{\partial t} + u \frac{\partial T}{\partial x} + v \frac{\partial T}{\partial y} = \alpha_{nf} \frac{\partial^2 T}{\partial y^2} \quad (15)$$

where t represent the time. Using the variables τ and (6), the new similarity solutions are:

$$\eta = \left(\frac{U}{v_f x} \right)^{\frac{1}{2}} y, \psi = (v_f x U)^{\frac{1}{2}} f(\eta, \tau), \theta(\eta, \tau) = \frac{T - T_\infty}{T_w - T_\infty}, \tau = \frac{U}{x} t \quad (16)$$

Equations (14) and (15) can be written as:

$$\frac{1}{(1-\varphi)^{2.5} (1-\varphi + \varphi \rho_{CNT}/\rho_f)} \frac{\partial^3 f}{\partial \eta^3} + \frac{1}{2} f \frac{\partial^2 f}{\partial \eta^2} + \tau \left(\frac{\partial f}{\partial \eta} \frac{\partial^2 f}{\partial \eta \partial \tau} - \frac{\partial f}{\partial \tau} \frac{\partial^2 f}{\partial \eta^2} \right) - \frac{\partial^2 f}{\partial \eta \partial \tau} = 0 \quad (17)$$

$$\frac{1}{\text{Pr} \left[1 - \varphi + \varphi (\rho C_p)_{CNT} / (\rho C_p)_f \right]} \frac{\partial^2 \theta}{\partial \eta^2} + \frac{1}{2} f \frac{\partial \theta}{\partial \eta} + \tau \left(\frac{\partial f}{\partial \eta} \frac{\partial \theta}{\partial \tau} - \frac{\partial f}{\partial \tau} \frac{\partial \theta}{\partial \eta} \right) - \frac{\partial \theta}{\partial \tau} = 0 \quad (18)$$

the new constrictions are now replaced by:

$$f(0, \tau) = 0, \frac{\partial f}{\partial \eta}(0, \tau) = \lambda + \sigma \frac{\partial^2 f}{\partial \eta^2}(0, \tau), \theta(0, \tau) = 1 \quad (19)$$

$$\frac{\partial f}{\partial \eta}(\eta, \tau) \rightarrow 1 - \lambda, \theta(\eta, \tau) \rightarrow 0 \text{ as } \eta \rightarrow \infty$$

To identify the stability solution $f(\eta) = f_0(\eta)$ and $\theta(\eta) = \theta_0(\eta)$ fulfilling the boundary-value problem as in Equations (7)–(9), we introduced the following term (see [28]):

$$f(\eta, \tau) = f_0(\eta) + e^{-\gamma \tau} F(\eta, \tau), \theta(\eta, \tau) = \theta_0(\eta) + e^{-\gamma \tau} G(\eta, \tau) \quad (20)$$

where $F(\eta, \tau)$ and $G(\eta, \tau)$ are small relative to $f_0(\eta)$ and $\theta_0(\eta)$ and γ is an unknown eigenvalue. Substitute Equations (20) into Equations (17)–(19), we get the following linearized problem:

$$\frac{1}{(1-\varphi)^{2.5} (1-\varphi + \varphi \rho_{CNT}/\rho_f)} \frac{\partial^3 F}{\partial \eta^3} + \frac{1}{2} \left(f_0 \frac{\partial^2 F}{\partial \eta^2} + \frac{\partial^2 f_0}{\partial \eta^2} F \right) + \gamma \frac{\partial F}{\partial \eta} - \frac{\partial^2 F}{\partial \eta \partial \tau} = 0 \quad (21)$$

$$\frac{1}{\text{Pr} \left[1 - \varphi + \varphi (\rho C_p)_{CNT} / (\rho C_p)_f \right]} \frac{\partial^2 G}{\partial \eta^2} + \frac{1}{2} \left(f_0 \frac{\partial G}{\partial \eta} + \frac{\partial \theta_0}{\partial \eta} F \right) + \gamma G - \frac{\partial G}{\partial \tau} = 0 \quad (22)$$

subject to the boundary conditions:

$$F(0, \tau) = -2\tau \left(\gamma F(0, \tau) - \frac{\partial F}{\partial \tau}(0, \tau) \right) = 0, \frac{\partial F}{\partial \eta}(0, \tau) = \sigma \frac{\partial^2 F}{\partial \eta^2}(0, \tau), G(0, \tau) = 0 \quad (23)$$

$$\frac{\partial F}{\partial \eta}(\eta, \tau) \rightarrow 0, G(\eta, \tau) \rightarrow 0 \text{ as } \eta \rightarrow \infty$$

To find the initial growth or decay of the solutions (21) and (20) which were proposed by Weidman et al. [28], the stability of steady flow $f_0(\eta)$ and $\theta_0(\eta)$ are investigated by setting $\tau = 0$.

Hence, $F(\eta) = F_0(\eta)$ and $G(\eta) = G_0(\eta)$. In this respect, by substituting Equation (20) into (21)–(23), we get the final equations in the following form:

$$\frac{1}{(1 - \varphi)^{2.5} (1 - \varphi + \varphi \rho_{CNT} / \rho_f)} F_0''' + \frac{1}{2} (f_0 F_0'' + f_0'' F_0) + \gamma F_0' = 0 \tag{24}$$

$$\frac{1}{Pr} \frac{k_{nf} / k_f}{[1 - \varphi + \varphi (\rho C_p)_{CNT} / (\rho C_p)_f]} G_0'' + \frac{1}{2} (f_0 G_0' + F_0 \theta_0') + \gamma G_0 = 0 \tag{25}$$

the boundary conditions in Equation (23) now reduced to:

$$\begin{aligned} F_0(0) = 0, F_0'(0) = \sigma F_0''(0), G_0(0) = 0 \\ F_0'(\eta) \rightarrow 0, G_0(\eta) \rightarrow 0 \text{ as } \eta \rightarrow \infty \end{aligned} \tag{26}$$

The stability of the dual solution obtained is determined by the smallest eigenvalue γ . The flow of a solution is said to be stable if the smallest eigenvalue γ is positive ($\gamma \geq 0$) i.e., there is an initial decay of perturbation. However, when γ is negative ($\gamma < 0$), there is an initial growth of perturbation and thus we can conclude that the flow is in an unstable mode. Following Harris et al. [30], the smallest eigenvalues can be identified by relaxing a boundary condition on $F_0(\eta)$. Therefore, for the current work, we relax the boundary condition $F_0' \rightarrow 0$ as $\eta \rightarrow \infty$ and replace it with updated boundary condition $F_0''(0) = 1$.

4. Results and Discussion

The system of Equations (7) and (8) together with conditions in (9) are solved numerically using the bvp4c package in Matlab. Kierzenka and Shampine [33] introduced this function as a way to solve a two-point boundary value problems for ordinary differential equations. The numerical result was validated by comparing the present results with the results in the existing literature [11,14,17] for the case of a boundary layer with the absence of CNTs and slip ($\varphi = \sigma = 0$).

As can be seen from Table 2, the comparison shows close agreement between the present results and those available in the literature [11,14,17] and thus we are assured that the present numerical method is accurate. For future references, the values of reduced skin friction $f''(0)$ for $\varphi \neq 0$ are also included in Table 2. The effects of dimensionless governing parameter such as slip parameter, velocity parameter and nanoparticle volume fraction on velocity, temperature, skin friction coefficient and Nusselt number are investigated and illustrated graphically. The range of nanoparticle volume fraction φ is considered from 0 to 0.2 ($0 < \varphi < 0.2$), where $\varphi = 0$ is corresponding to the regular fluid.

Table 2. Values of $f''(0)$ for selected value of φ and λ for water-SWCNT and $\sigma = 0$.

| φ | λ | Blasius [11] | Sakiadis [14] | Bachok et al. [17] Solution | | Present Result Solution | |
|-----------|-----------|--------------|---------------|-----------------------------|--------|-------------------------|--------|
| | | | | First | Second | First | Second |
| 0 | −0.5 | | | 0.3979 | 0.1710 | 0.3978 | 0.1710 |
| | −0.4 | | | 0.4357 | 0.0834 | 0.4356 | 0.0834 |
| | −0.3 | | | 0.4339 | 0.0367 | 0.4339 | 0.0367 |
| | −0.2 | | | 0.4124 | 0.0114 | 0.4124 | 0.0114 |
| | −0.1 | | | 0.3774 | 0.0010 | 0.3774 | 0.0011 |
| | 0 | 0.332 | | 0.3321 | | 0.3321 | |
| | 0.5 | | | 0 | | 0 | |
| 0.1 | 1 | | −0.44375 | −0.4438 | | −0.4438 | |
| | −0.5 | | | | | 0.3757 | 0.1615 |
| | −0.4 | | | | | 0.4114 | 0.0787 |
| | −0.3 | | | | | 0.4098 | 0.0345 |
| | −0.2 | | | | | 0.3895 | 0.0107 |
| | −0.1 | | | | | 0.3564 | 0.0010 |
| | 0 | | | | | 0.3136 | |
| 0.5 | | | | | 0 | | |

Table 2. Cont.

| φ | λ | Blasius [11] | Sakiadis [14] | Bachok et al. [17] Solution | | Present Result Solution | |
|-----------|-----------|--------------|---------------|-----------------------------|--------|-------------------------|--------|
| | | | | First | Second | First | Second |
| 0.2 | 1 | | | | | -0.4191 | |
| | -0.5 | | | | | 0.3460 | 0.1488 |
| | -0.4 | | | | | 0.3789 | 0.0725 |
| | -0.3 | | | | | 0.3774 | 0.0307 |
| | -0.2 | | | | | 0.3587 | 0.0099 |
| | -0.1 | | | | | 0.3282 | 0.0000 |
| | 0 | | | | | 0.2888 | |
| | 0.5 | | | | | 0 | |
| | 1 | | | | | -0.3861 | |

Figures 2 and 3 illustrate the behaviors of nanoparticle volume fraction φ on the variation of reduced skin friction $f''(0)$ and reduced heat transfer $-\theta'(0)$ for water-SWCNTs. From these figures, it can be seen that there exist dual solutions when $\lambda_c < \lambda < 0$, i.e., opposing flow, while a unique solution exists when $\lambda \geq 0$. However, no solutions are found to exist when $\lambda < \lambda_c$, which means that there is a boundary layer separation and boundary layer approximations are not physically realizable. The variation of λ_c has been shown in Table 3, where the results are in good agreement with Bachok et al. [21] when $\varphi = 0$. From the figures, we can conclude that an increase of nanoparticles volume fraction φ causes the skin friction to decrease whereas the heat transfer rate at the surface increases. This is because nanofluids become more viscous by adding CNTs and this also enhances their thermal conductivity.

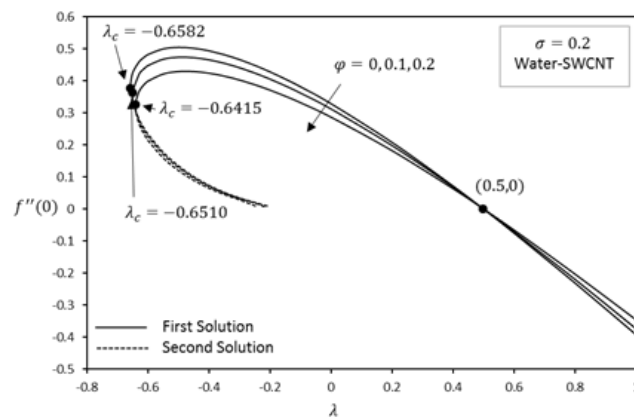


Figure 2. Effect of φ on reduced skin friction $f''(0)$.

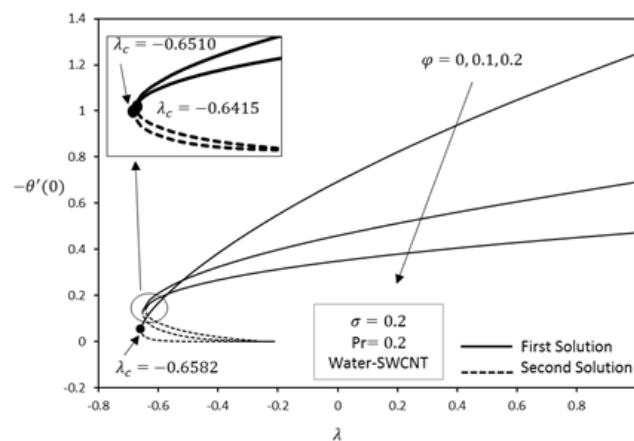


Figure 3. Effect of φ on reduced heat transfer $-\theta'(0)$.

Table 3. Variation of λ_c with $\sigma = 0.2$ and water-SWCNT for different value of φ .

| φ | Bachok et al. [21] | Present Result |
|-----------|--------------------|----------------|
| 0 | -0.6582 | -0.6582 |
| 0.1 | | -0.6510 |
| 0.2 | | -0.6415 |

Figures 4 and 5 show the effect of slip parameter on reduced skin friction $f''(0)$ and reduced heat transfer $-\theta'(0)$. It is observed that for no-slip boundary conditions, i.e., $\sigma = 0$, the similarity solution exists only when $\lambda \geq \lambda_c = -0.5482$. When the slip at the boundary increases, i.e., $\sigma = 0.1$ the range of λ values where solutions exist becomes larger ($\lambda \geq \lambda_c = -0.6480$). For further increment in the slip parameter, $\sigma = 0.2$ the range of $\lambda \geq \lambda_c = -0.7910$, respectively, so the analysis implies that with the increase in slip parameter σ , the reduced skin friction and heat loss from the surface increases. It is further observed that when the slip takes place in the boundary layer, there will be more resistance between the fluid and plate that cause the solution existence range to increase, hence postponing the boundary layer separation and this increment happens in the range where dual solutions exist. Moreover, it is noticed that for a fixed velocity ratio parameter, the value of the reduced skin friction and reduced heat transfer increases with an increase of slip parameter in the first solution and decreases in the second solution.

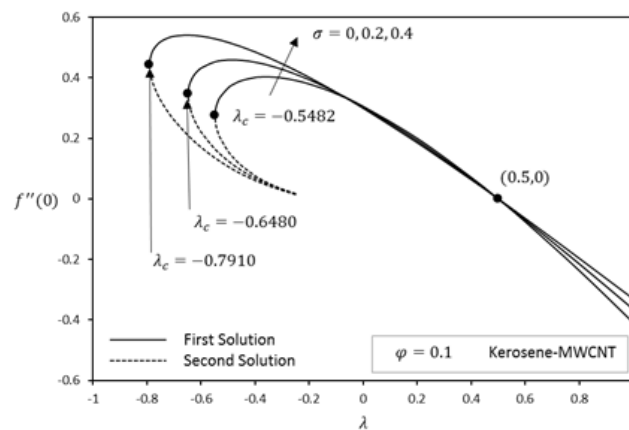


Figure 4. Effect of σ on reduced skin friction $f''(0)$.

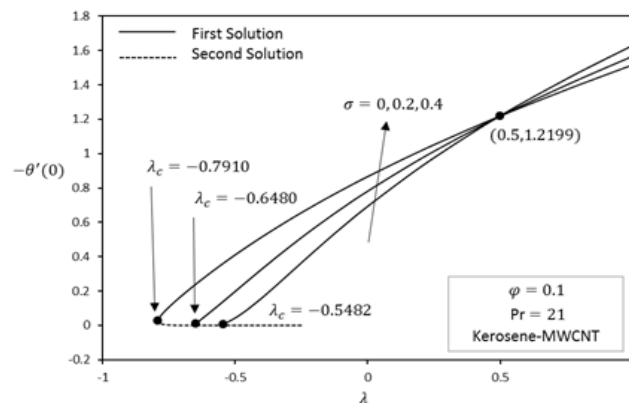


Figure 5. Effect of σ on reduced heat transfer $-\theta'(0)$.

The effect of skin friction and Nusselt numbers are investigated and shown in Figures 6–17. It can be clearly seen that the value of these quantities increases almost linearly with nanoparticle volume fraction. Figures 6–8 shows the variation of slip parameter on the skin friction coefficient for different base fluids (water and kerosene) and considering both SWCNTs and MWCNTs. When the plate moves

in the same direction as the free stream, the skin friction coefficient decreases with an increase in slip parameter. Figures 9–11 depict the numerical values of the skin friction with volume fraction of CNTs when the plate moves in an assisting flow for both SWCNTs and MWCNTs. It is observed that the skin friction decreases with an increase in the plate velocity. However, the skin friction of SWCNTs is found to be higher compared to MWCNTs. The density of SWCNTs is found to be higher than that of MWCNTs (Table 1). Further, skin friction is higher in kerosene oil compared to water.

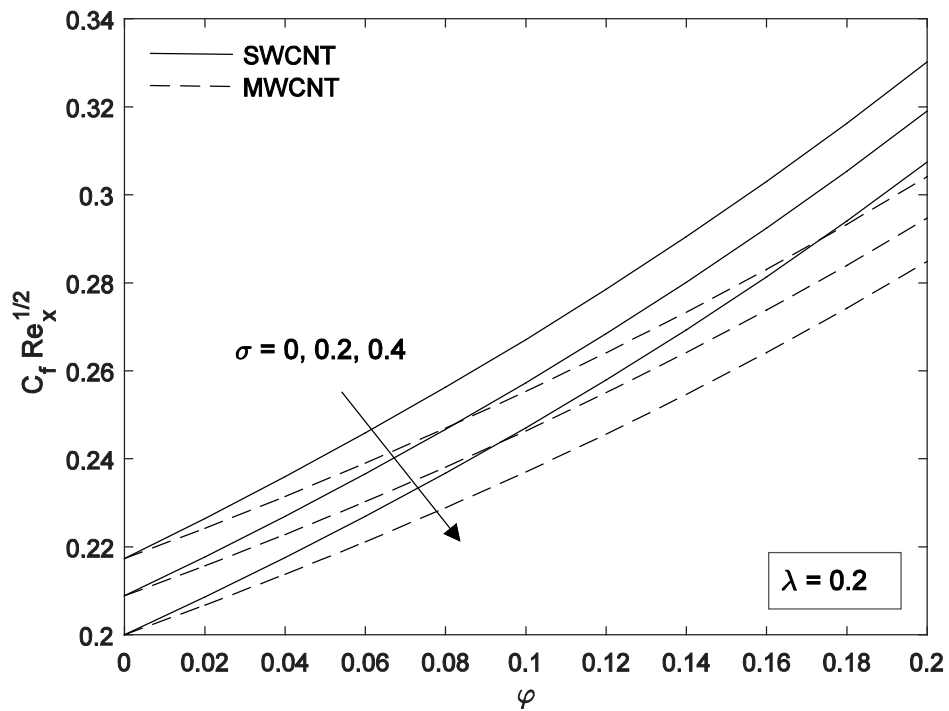


Figure 6. Effect of σ on skin friction for water-based fluid.

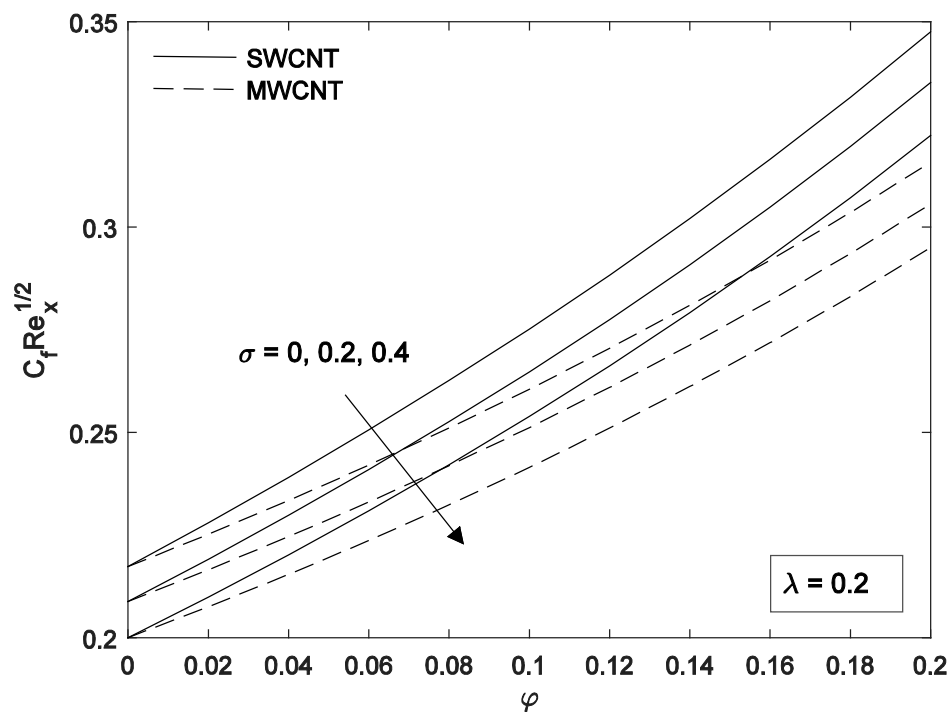


Figure 7. Effect of σ on skin friction for kerosene-based fluid.

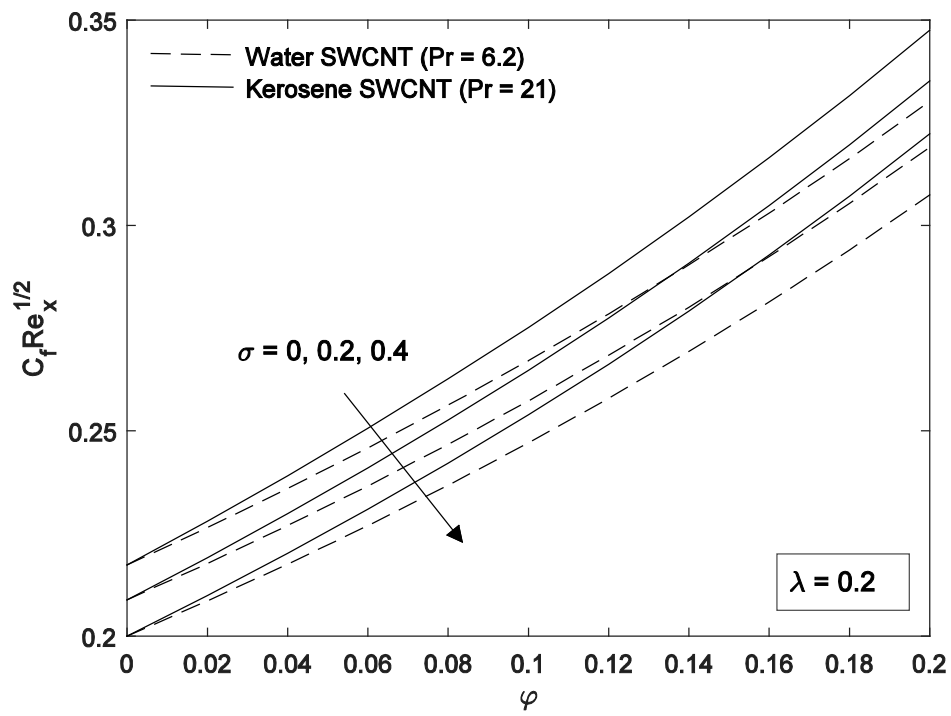


Figure 8. Effect of σ on skin friction for water-kerosene based fluid.

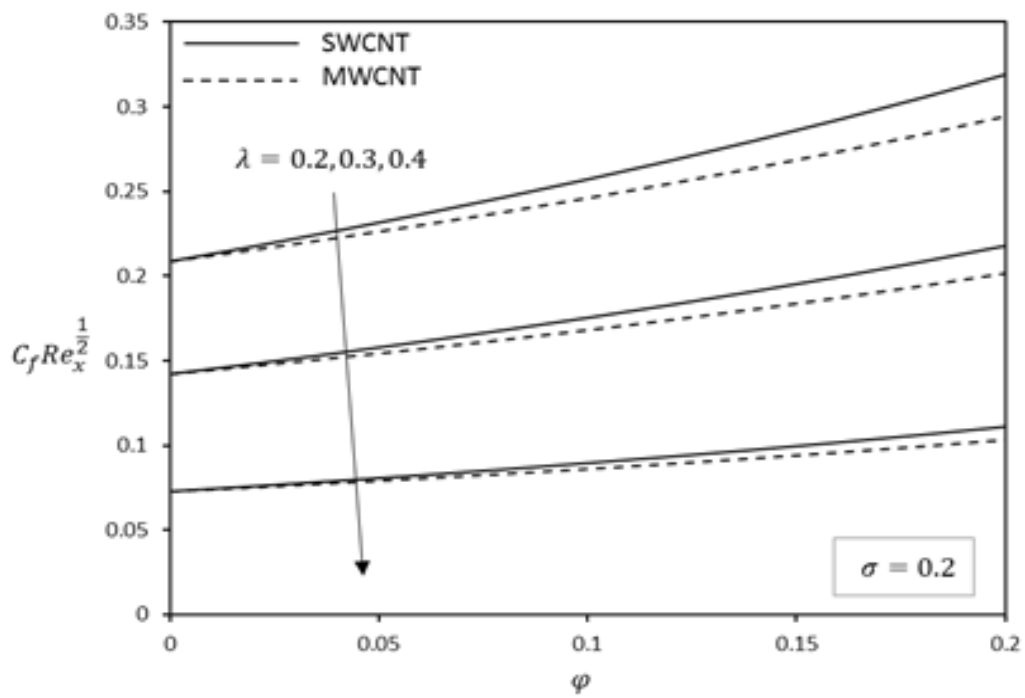


Figure 9. Effect of λ on skin friction for water-based fluid.

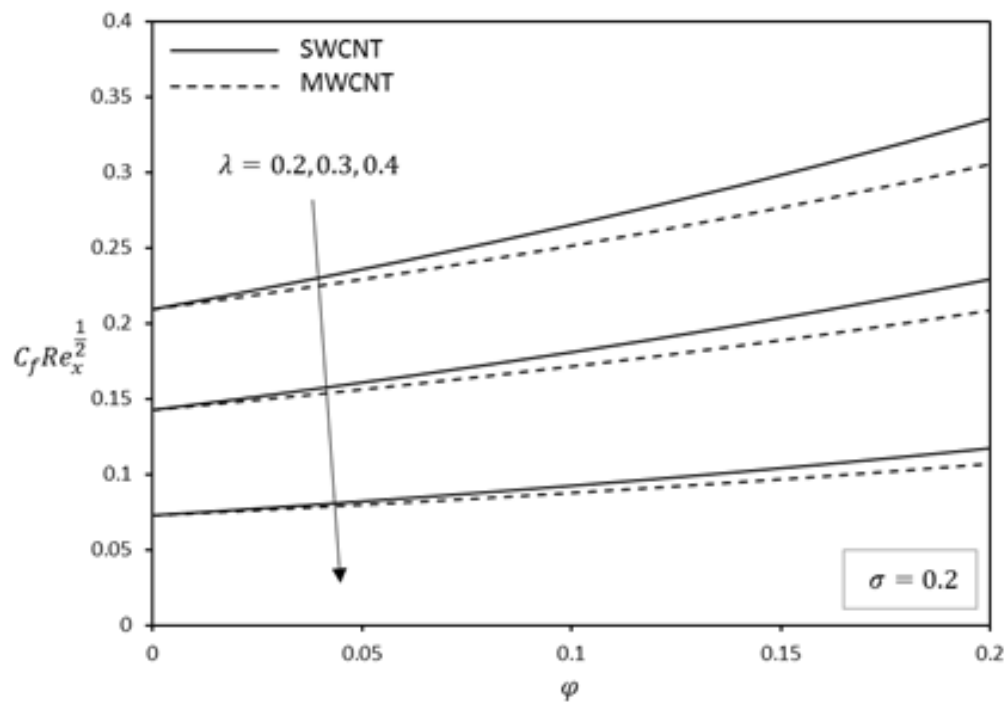


Figure 10. Effect of λ on skin friction for kerosene-based fluid.

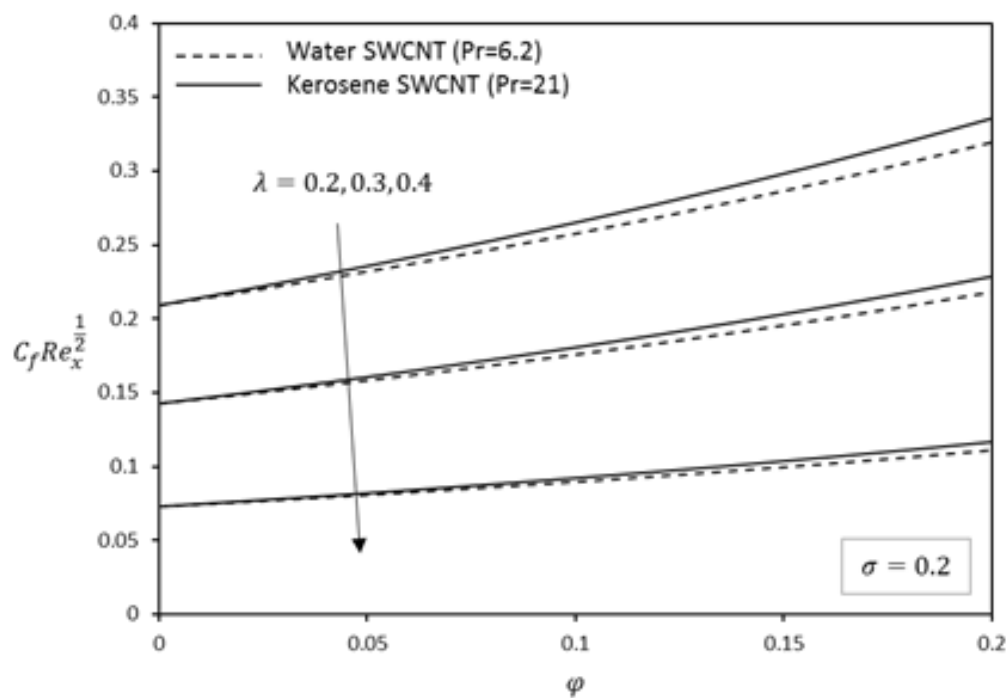


Figure 11. Effect of λ on skin friction for water-kerosene based fluid.

The effect of the slip parameter on the variation of Nusselt numbers with volume fraction of CNTs is reported in Figures 12–14 for different base fluids (water and kerosene) and considering both SWCNTs and MWCNTs. It is revealed that the Nusselt number increases with an increase in slip parameter. The present of slip also improves the convective heat transfer at the surface. Figures 15–17 shows the influence of plate velocity on Nusselt number for both SWCNTs and MWCNTs. When the plate moves in the direction of the free stream, the Nusselt number increases with an increase in the plate velocity of both CNTs. Due to their higher thermal conductivity, SWCNTs possess higher

Nusselt numbers in each case. Again, we found that kerosene oil has a higher Nusselt number compared to water. The nanofluids having a higher concentration of CNTs causes higher viscosity. In addition, carbon nanotubes have a great contribution in the flow motion of nanofluid and in the heat transfer application.

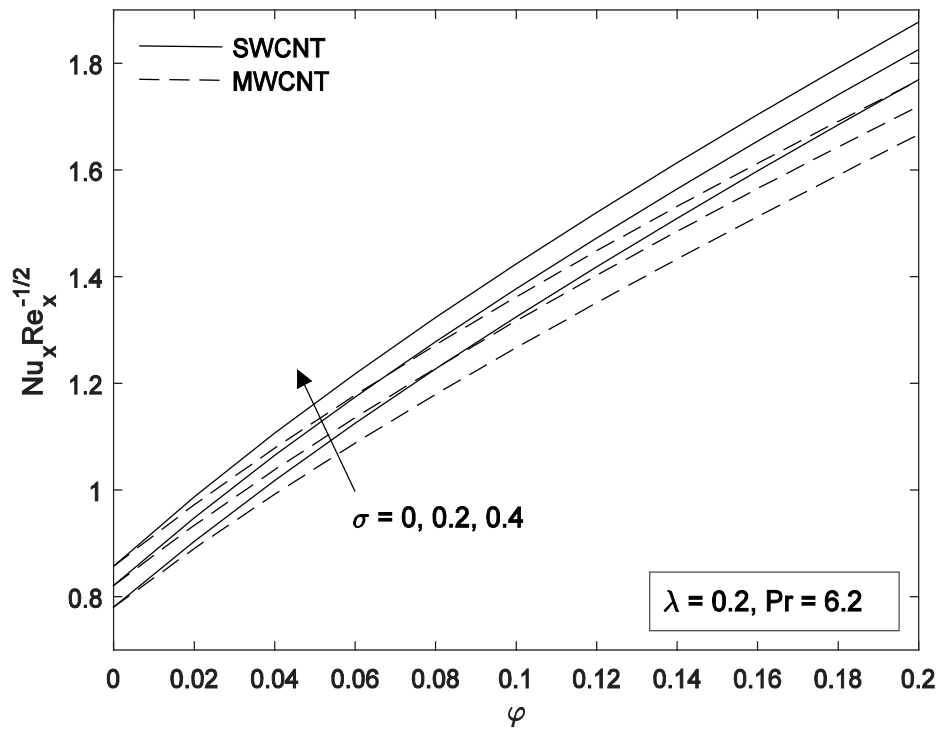


Figure 12. Effect of σ on Nusselt number for water-based fluid.

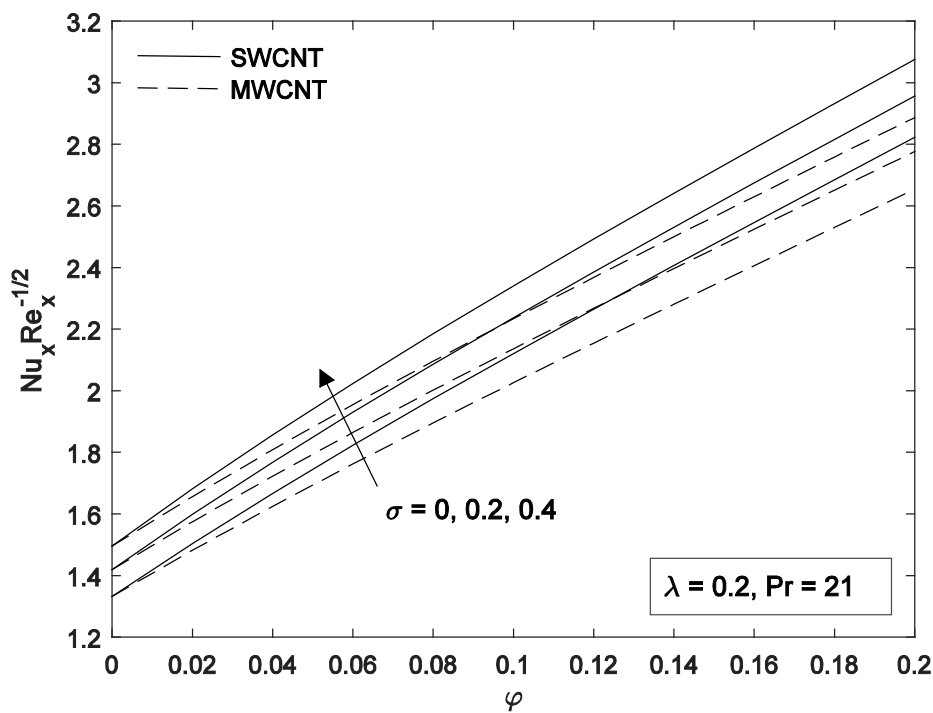


Figure 13. Effect of σ on Nusselt number for kerosene-based fluid.

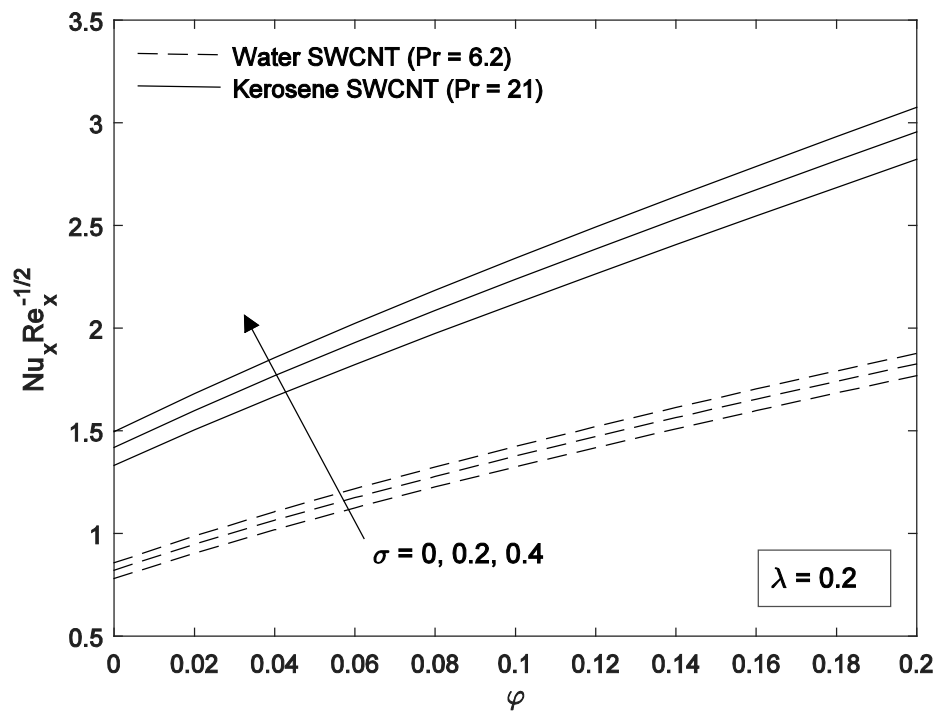


Figure 14. Effect of σ on Nusselt number for water-kerosene based fluid.

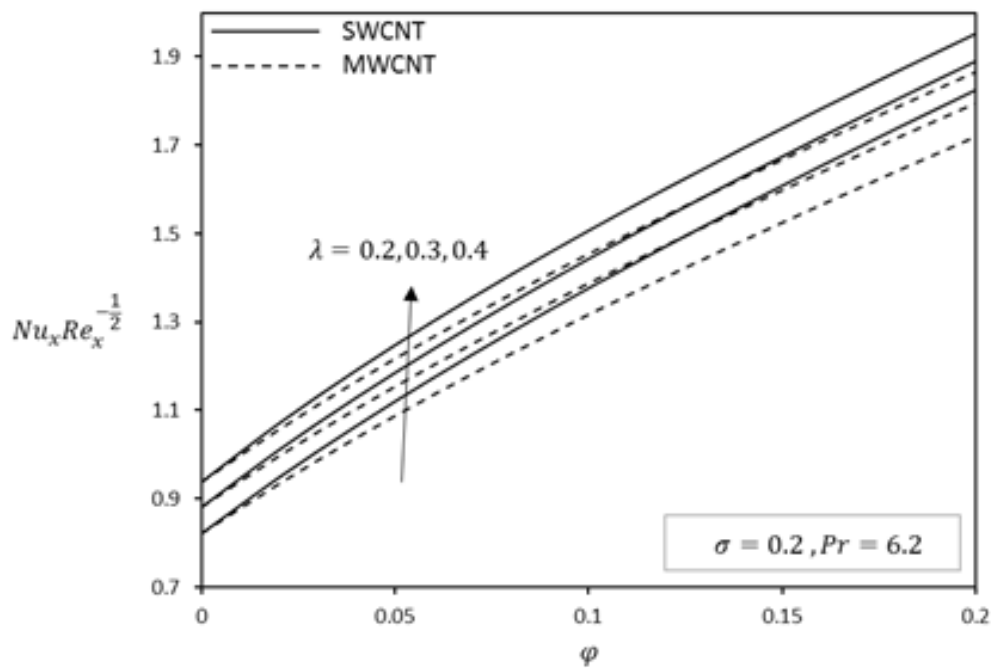


Figure 15. Effect of λ on Nusselt number for water-based fluid.

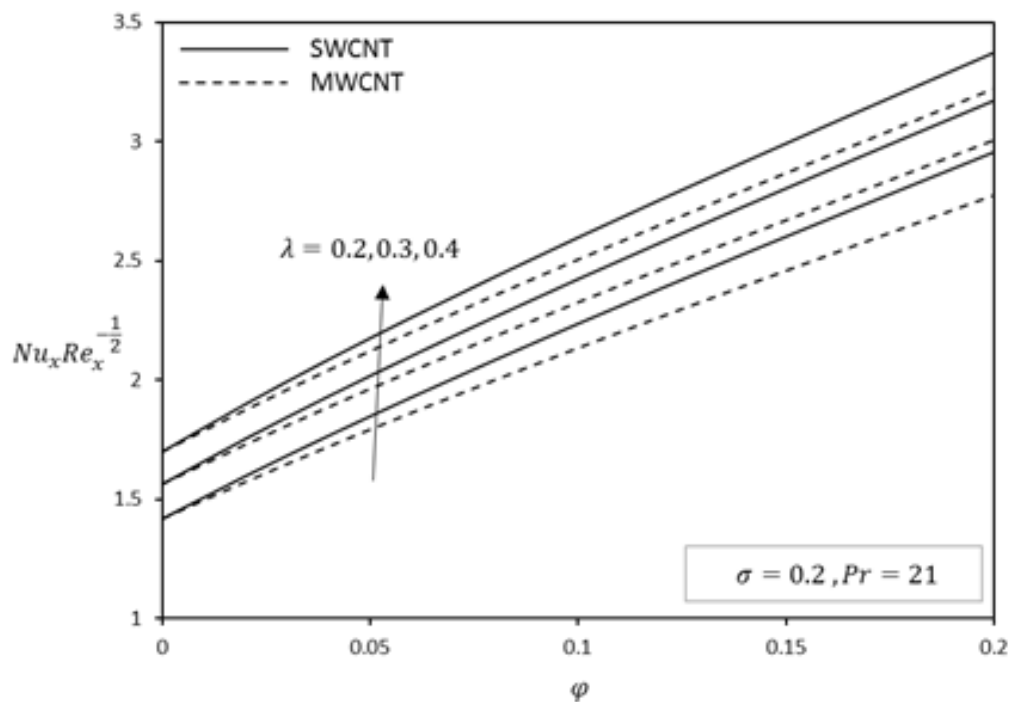


Figure 16. Effect of λ on Nusselt number for kerosene-based fluid.

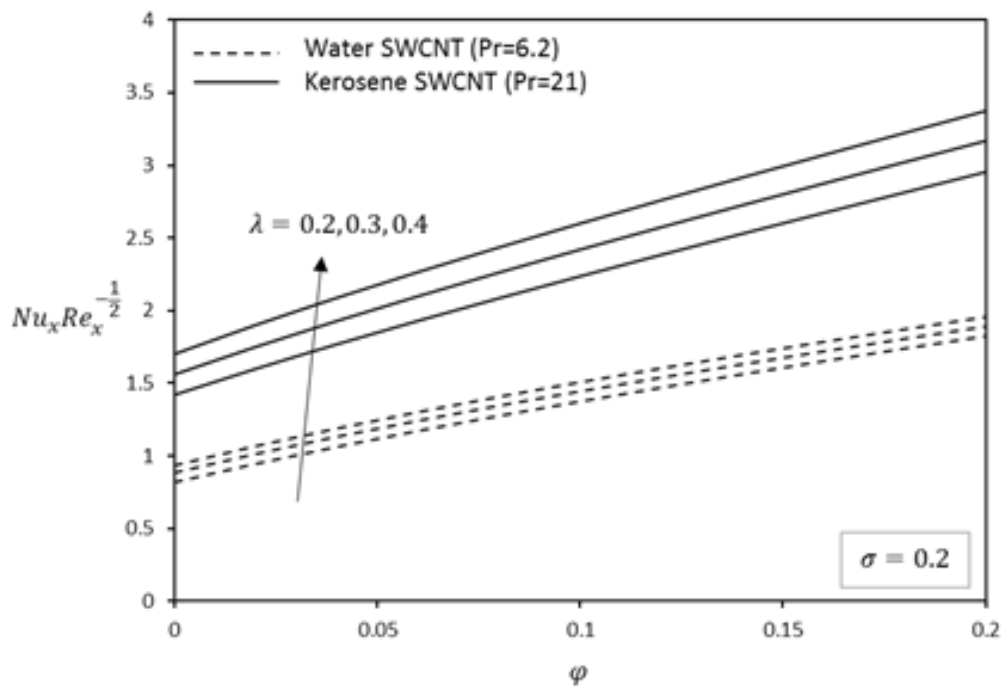


Figure 17. Effect of λ on Nusselt number for water-kerosene based fluid.

These numerical solutions and dual solution obtained were graphically supported and validated by the velocity and temperature profile plotted in Figures 18–23. These profiles satisfy the boundary conditions (9) and converge asymptotically. The dual solutions can be clearly seen from the figures. It is also clearly observed that the first solution has a thinner boundary layer thickness compared to second solution. Variations of velocity $f'(\eta)$ and temperature $\theta(\eta)$ profiles for different volume fractions of CNTs are presented in Figures 18 and 19, respectively, for water-based SWCNTs. It is found that the velocity of fluid is decrease in both solution when the CNT volume fraction increases. We can

also observe that temperature profile increases with an increase of CNT volume fraction. The addition of sufficient nanoparticles can enhance the temperature of the fluid quite significantly due to the very high thermal conductivity of carbon nanotubes compared to other nanoparticles.

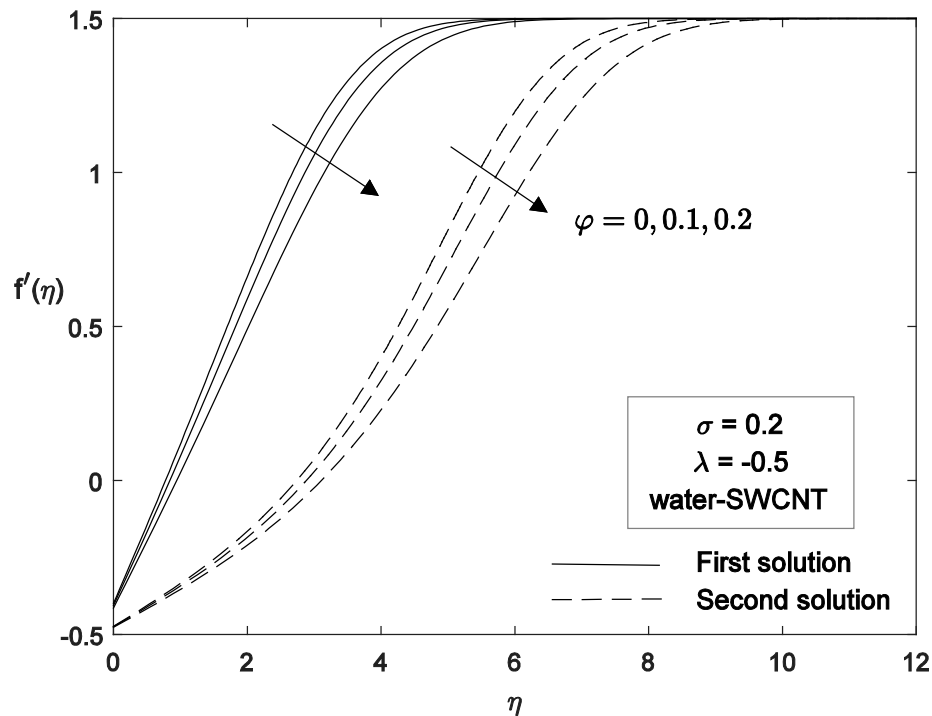


Figure 18. Effect of various φ on velocity profile.

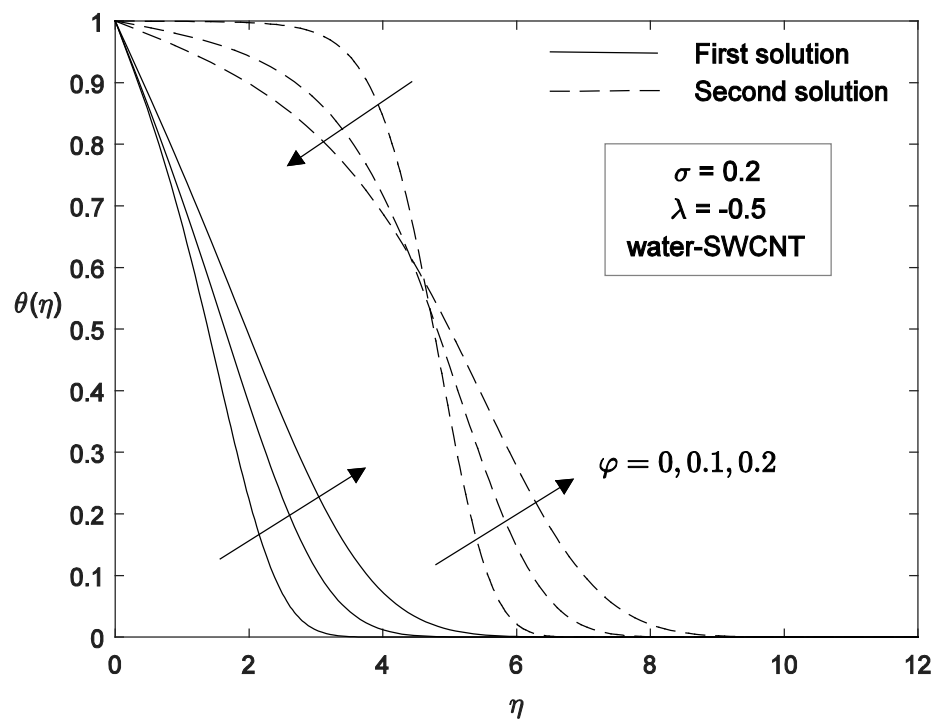


Figure 19. Effect of various φ on temperature profile.

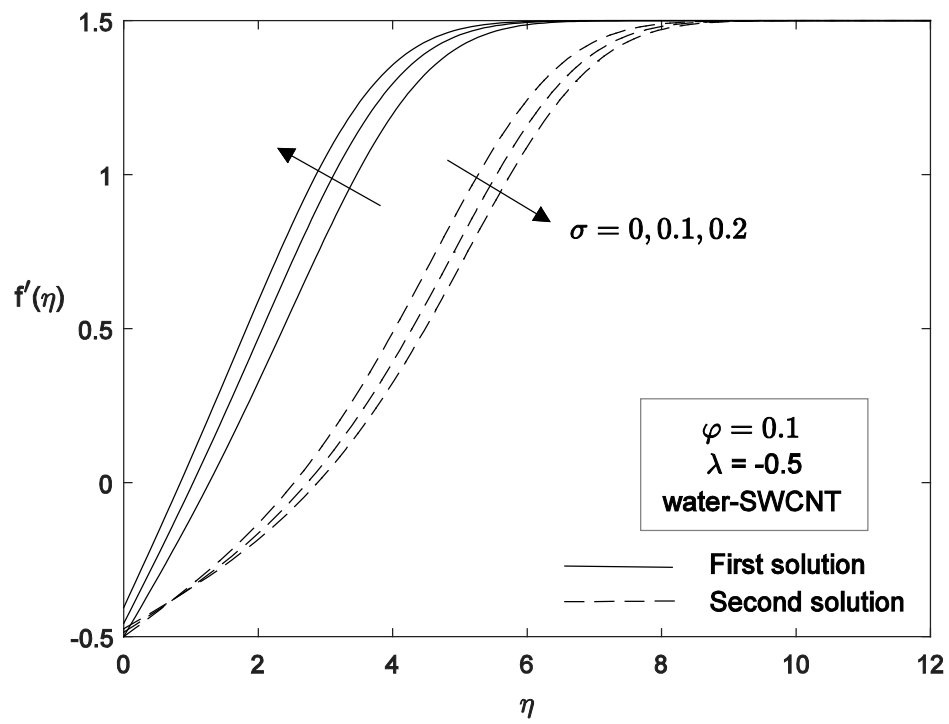


Figure 20. Effect of various σ on velocity profile.

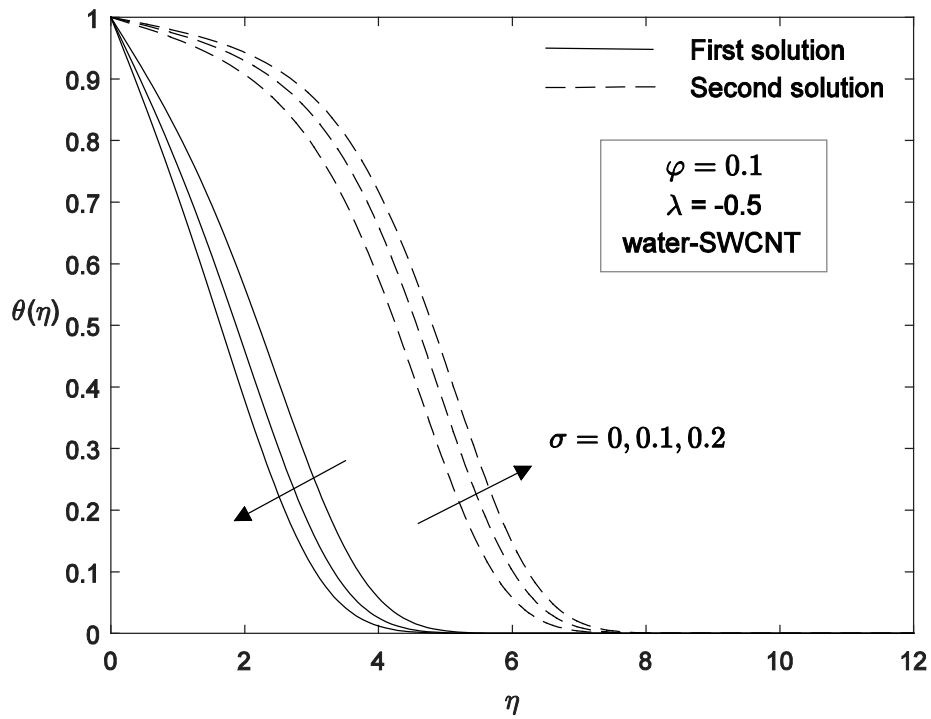


Figure 21. Effect of various σ on temperature profile.

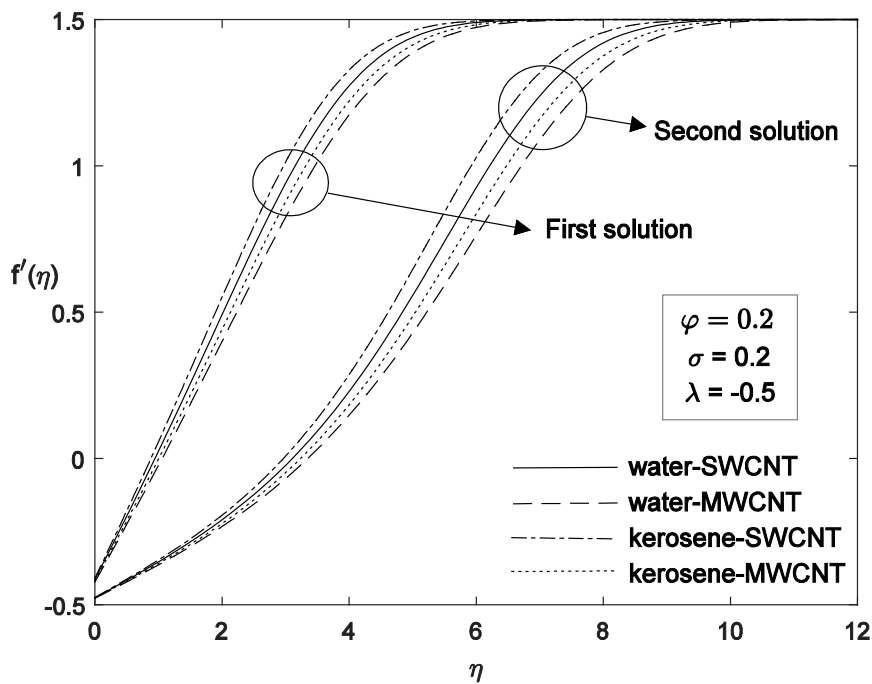


Figure 22. Effect of various nanoparticles on velocity profile.

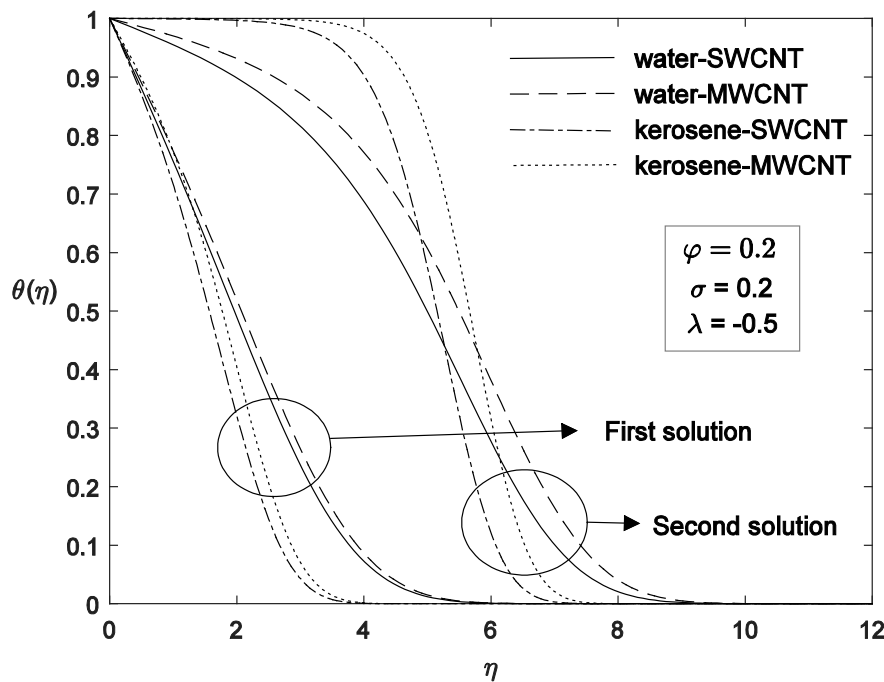


Figure 23. Effect of various nanoparticles on temperature profile.

Meanwhile in Figures 20 and 21, the dual velocity and temperature profiles show that with an increase of slip parameter, the velocity profile increases in the first solution and decreases in the second solution. Meanwhile, the temperature profile is found to decrease with an increase of slip parameter. It is noticed that kerosene-SWCNT has higher velocity and temperature compared to others in Figures 22 and 23.

A stability analysis is conducted numerically in MATLAB software by using a bvp4c function to determine the stability of solutions obtained in this recent work. The set of ordinary differential Equations (24) and (25) subjected to the new boundary condition (26) is used to find the smallest

eigenvalue γ . The smallest eigenvalue γ for some values of φ and λ when $\sigma = 0.2$ are presented in Table 4. It is observed that the first solution shows a positive smallest eigenvalues, while the second solution shows a negative smallest eigenvalues. The smallest eigenvalue is drawn closer to zero ($\gamma \rightarrow 0$) as λ is approaching the critical point λ_c either from positive or negative sign. We can finally conclude that the first solution was linearly stable and physically realizable while the second solution was an unstable solution.

Table 4. Smallest eigenvalues γ at selected values of φ and λ for different nanoparticle when $\sigma = 0.2$.

| Nanoparticles | φ | λ | First Solution | Second Solution |
|---------------|-----------|-----------|----------------|-----------------|
| Water-SWCNT | 0 | −0.658 | 0.0069 | −0.0067 |
| | | −0.65 | 0.0383 | −0.0340 |
| | | −0.6 | 0.1092 | −0.0784 |
| | 0.1 | −0.6509 | 0.0051 | −0.0050 |
| | | −0.65 | 0.0133 | −0.0127 |
| | | −0.6 | 0.1020 | −0.0746 |
| | | −0.641 | 0.0098 | −0.0095 |
| | 0.2 | −0.64 | 0.0163 | −0.0155 |
| | | −0.6 | 0.0917 | −0.0689 |
| | | −0.635 | 0.0663 | −0.0540 |
| Water-MWCNT | 0 | −0.63 | 0.0736 | −0.0587 |
| | | −0.6 | 0.1092 | −0.0784 |
| | | −0.645 | 0.0110 | −0.0106 |
| | 0.1 | −0.64 | 0.0318 | −0.0287 |
| | | −0.6 | 0.0963 | −0.0715 |
| | | −0.633 | 0.0037 | −0.0037 |
| | | −0.63 | 0.0232 | −0.0215 |
| | 0.2 | −0.6 | 0.0813 | −0.0629 |

5. Conclusions

We have studied the flow and heat transfer characteristics of carbon nanotubes (single-wall and multi-wall carbon nanotube) in different base fluids for a moving flat plate. It is concluded that:

- The skin friction decreases with an increase of carbon nanotubes volume fraction, whereas the heat transfer rate increases.
- Single-wall CNTs are more efficient than multi-wall CNTs in skin friction and heat transfer rate.
- Kerosene-based CNTs have higher skin friction and heat transfer rates than water-based CNTs.
- The range of solutions widely expanded with an increment of slip parameter.
- For the opposing flow, slip parameter increases the skin friction coefficient and heat transfer.
- The existence of unique solutions occurs when the plate moves in the same direction ($\lambda > 0$) whereas dual solutions occur when the plate move in the opposite direction ($\lambda_c < \lambda < 0$).
- The first solution was a stable solution and physically relevant, while the second solution was an unstable solution.

Author Contributions: conceptualization, N.S.A., N.B.; methodology, software and formal analysis, N.S.A.; validation, N.B., I.P.; writing—original draft preparation, N.S.A.; writing—review and editing, N.B., I.P.; supervision, N.B.

Acknowledgments: The authors gratefully acknowledge the financial support received in the form of a fundamental research grant scheme (FRGS/1/2018/STG06/UPM/02/4) and My BrainSc from the Ministry of Higher Education, Malaysia. The work of I. Pop has been supported from the grant PN-III-P4-ID-PCE-2016-0036, UEFISCDI, Romania. Lastly, a humble yet sincere gratitude to all the reviewers for their honest feedback and suggestions.

Conflicts of Interest: The authors declare no conflict of interest.

References

1. Das, S.K.; Choi, S.U.; Yu, W.; Pradeep, T. *Nanofluids: Science and Technology*; John Wiley & Sons: Hoboken, NJ, USA, 2007.
2. Chol, S.U.S.; Estman, J.A. Enhancing thermal conductivity of fluids with nanoparticles. *ASME Publ. -Fed* **1995**, *231*, 99–106.
3. Halelfadl, S.; Maré, T.; Estellé, P. Efficiency of carbon nanotubes water based nanofluids as coolants. *Exp. Therm. Fluid Sci.* **2014**, *53*, 104–110. [[CrossRef](#)]
4. Choi, S.U.S.; Zhang, Z.G.; Yu, W.; Lockwood, F.E.; Grulke, E.A. Anomalous thermal conductivity enhancement in nanotube suspensions. *Appl. Phys. Lett.* **2001**, *79*, 2252–2254. [[CrossRef](#)]
5. Maré, T.; Halelfadl, S.; Sow, O.; Estellé, P.; Duret, S.; Bazantay, F. Comparison of the thermal performances of two nanofluids at low temperature in a plate heat exchanger. *Exp. Therm. Fluid Sci.* **2011**, *35*, 1535–1543. [[CrossRef](#)]
6. Liu, M.S.; Lin, M.C.C.; Huang, I.T.; Wang, C.C. Enhancement of thermal conductivity with carbon nanotube for nanofluids. *Int. Commun. Heat Mass Transf.* **2005**, *32*, 1202–1210. [[CrossRef](#)]
7. Garg, P.; Alvarado, J.L.; Marsh, C.; Carlson, T.A.; Kessler, D.A.; Annamalai, K. An experimental study on the effect of ultrasonication on viscosity and heat transfer performance of multi-wall carbon nanotube-based aqueous nanofluids. *Int. J. Heat Mass Transf.* **2009**, *52*, 5090–5101. [[CrossRef](#)]
8. Xue, Q.Z. Model for thermal conductivity of carbon nanotube-based composites. *Phys. B Condens. Matter* **2005**, *368*, 302–307. [[CrossRef](#)]
9. Ding, Y.; Alias, H.; Wen, D.; Williams, R.A. Heat transfer of aqueous suspensions of carbon nanotubes (CNT nanofluids). *Int. J. Heat Mass Transf.* **2006**, *49*, 240–250. [[CrossRef](#)]
10. Kumaresan, V.; Velraj, R.; Das, S.K. Convective heat transfer characteristics of secondary refrigerant based CNT nanofluids in a tubular heat exchanger. *Int. J. Refrig.* **2012**, *35*, 2287–2296. [[CrossRef](#)]
11. Blasius, H. Grenzschichten in Flüssigkeiten mit kleiner Reibung. *Z. Angew. Math. Phys.* **1908**, *56*, 1–37.
12. Wang, L. A new algorithm for solving classical Blasius equation. *Appl. Math. Comput.* **2004**, *157*, 1–9. [[CrossRef](#)]
13. Cortell, R. Numerical solutions of the classical Blasius flat-plate problem. *Appl. Math. Comput.* **2005**, *170*, 706–710. [[CrossRef](#)]
14. Sakiadis, B.C. Boundary-layer behavior on continuous solid surfaces: I. Boundary-layer equations for two-dimensional and axisymmetric flow. *AIChE J.* **1961**, *7*, 26–28. [[CrossRef](#)]
15. Ishak, A.; Nazar, R.; Pop, I. Flow and heat transfer characteristics on a moving flat plate in a parallel stream with constant surface heat flux. *Heat Mass Transf.* **2009**, *45*, 563–567. [[CrossRef](#)]
16. Ishak, A.; Nazar, R.; Pop, I. The effects of transpiration on the flow and heat transfer over a moving permeable surface in a parallel stream. *Chem. Eng. J.* **2009**, *148*, 63–67. [[CrossRef](#)]
17. Bachok, N.; Ishak, A.; Pop, I. Flow and heat transfer characteristics on a moving plate in a nanofluid. *Int. J. Heat Mass Transf.* **2012**, *55*, 642–648. [[CrossRef](#)]
18. Bhattacharyya, K.; Mukhopadhyay, S.; Layek, G.C. MHD boundary layer slip flow and heat transfer over a flat plate. *Chin. Phys. Lett.* **2011**, *28*, 024701. [[CrossRef](#)]
19. Bhattacharyya, K.; Mukhopadhyay, S.; Layek, G.C. Steady boundary layer slip flow and heat transfer over a flat porous plate embedded in a porous media. *J. Pet. Sci. Eng.* **2011**, *78*, 304–309. [[CrossRef](#)]
20. Bhattacharyya, K.; Layek, G.C.; Gorla, R.S.R. Slip effect on boundary layer flow on a moving flat plate in a parallel free stream. *Int. J. Fluid Mech. Res.* **2012**, *39*. [[CrossRef](#)]
21. Bachok, N.; Najib, N.; Arifin, N.M.; Senu, N. Stability of dual solution boundary layer flow and heat transfer on a moving plate in a copper-water nanofluid with slip effect. *WSEAS Trans. Fluid Mech.* **2016**, *11*, 151–158. [[CrossRef](#)]
22. Khan, W.A.; Khan, Z.H.; Rahi, M. Fluid flow and heat transfer of carbon nanotubes along a flat plate with Navier slip boundary. *Appl. Nanosci.* **2014**, *4*, 633–641. [[CrossRef](#)]
23. Imtiaz, M.; Hayat, T.; Alsaedi, A.; Ahmad, B. Convective flow of carbon nanotubes between rotating stretchable disks with thermal radiation effects. *Int. J. Heat Mass Transf.* **2016**, *101*, 948–957. [[CrossRef](#)]
24. Hayat, T.; Haider, F.; Muhammad, T.; Alsaedi, A. Three dimensional rotating flow of carbon nanotubes with Darcy-Forchheimer porous medium. *PLoS ONE* **2017**, *12*, e0179576. [[CrossRef](#)] [[PubMed](#)]

25. Hayat, T.; Hussain, Z.; Alsaedi, A.; Ahmad, B. Heterogeneous-homogeneous reactions and melting heat transfer effects in flow with carbon nanotubes. *J. Mol. Liq.* **2016**, *220*, 200–207. [[CrossRef](#)]
26. Sreedevi, P.; Reddy, P.S.; Chamka, A.J. Magneto-hydrodynamics heat and mass transfer analysis of single and multi-wall carbon nanotubes over vertical cone with convective boundary condition. *Int. J. Mech. Sci.* **2018**, *135*, 646–655. [[CrossRef](#)]
27. Merkin, J.H. On dual solutions occurring in mixed convection in a porous medium. *J. Eng. Math.* **1985**, *20*, 171–179. [[CrossRef](#)]
28. Weidman, P.D.; Kubitschek, D.G.; Davis, A.M.J. The effect of transpiration on self-similar boundary layer flow over moving surfaces. *Int. J. Eng. Sci.* **2006**, *44*, 730–737. [[CrossRef](#)]
29. Merrill, K.; Beauchesne, M.; Previte, J.; Paultet, J.; Weidman, P. Final steady flow near a stagnation point on a vertical surface in a porous medium. *Int. J. Heat Mass Transf.* **2006**, *49*, 4681–4686. [[CrossRef](#)]
30. Harris, S.D.; Ingham, D.B.; Pop, I. Mixed convection boundary-layer flow near the stagnation point on a vertical surface in a porous medium: Brinkman model with slip. *Transp. Porous Media* **2009**, *77*, 267–285. [[CrossRef](#)]
31. Oztop, H.F.; Abu-Nada, E. Numerical study of natural convection in partially heated rectangular enclosures filled with nanofluids. *In. J. Heat Fluid Flow* **2008**, *29*, 1326–1336. [[CrossRef](#)]
32. Afzal, N.; Badaruddin, A.; Elgarvi, A.A. Momentum and heat transport on a continuous flat surface moving in a parallel stream. *Int. J. Heat Mass Transf.* **1993**, *36*, 3399–3403. [[CrossRef](#)]
33. Kierzenka, J.; Shampine, L.F. A BVP solver based on residual control and the Matlab PSE. *ACM Trans. Math. Softw.* **2001**, *27*, 299–316. [[CrossRef](#)]



© 2018 by the authors. Licensee MDPI, Basel, Switzerland. This article is an open access article distributed under the terms and conditions of the Creative Commons Attribution (CC BY) license (<http://creativecommons.org/licenses/by/4.0/>).